

# Hyperfine Structures of Doxyl-Labeled *n*-Alkyl Chains by NMR and EPR

BARNEY L. BALES,\* DONNA MARENO,† AND FRANCIS L. HARRIS†

\* Department of Physics and Astronomy and The Center for Cancer and Developmental Biology and † Department of Chemistry, California State University, Northridge, California 91330

Received October 29, 1992; revised December 29, 1992

The proton hyperfine coupling constants in a series of *n*-alkyl chains with a doxyl group attached at various points from the end of the chain have been measured by NMR and EPR spectroscopies. The hyperfine structure shows no further change when the attachment point is four or more carbon-carbon bonds from the end of the chain. The high resolution afforded by 500 MHz NMR reveals small magnetic inequivalencies in the chain methylene hyperfine coupling constants located at the same distance from the attachment point. Protons in the same chain methylene group are shown to have different hyperfine coupling constants while protons on different chain methylene groups, symmetrically placed with respect to attachment point, are the same, in every case except one. EPR spectra simulated from hyperfine coupling constants derived from NMR are in excellent agreement with experiment. Inhomogeneous EPR line broadening is found to be in excellent agreement with a previously derived universal hyperfine pattern (B. L. Bales, in "Biological Magnetic Resonance" (L. J. Berliner and J. Reuben, Eds.), Vol. 8, p. 77, Plenum, New York, 1989), so no new correction procedures are necessary. Strategies for selectively deuterating *n*-alkyl spin probes are developed and compared with some results taken from the literature. Deuterating the chain methylene groups two to three carbon-carbon bonds from the attachment point is necessary for the maximum gain in resolution and sensitivity. © 1993 Academic Press, Inc.

## INTRODUCTION

Hyperfine interactions are prominent in nitroxide free radicals (1). The hyperfine structures of many of these radicals important in EPR spin probe studies have been established by NMR (2–8) and confirmed or corrected (9, 10) by EPR. Much of this structure is unresolved in most EPR experiments, but plays an important role because it inhomogeneously broadens the resonance lines. Detailed knowledge of the structure is often not necessary to correct for inhomogeneous broadening, but it sometimes is (11); additionally, rational approaches to selective deuteration to reduce the inhomogeneous broadening require detailed knowledge. A recent review (1) summarizes the known hyperfine structures and details methods to correct the effect of that structure on various parameters in spin probe research. One of the most important classes of spin probes,

doxyl-labeled *n*-alkyl chains, was conspicuously absent in that review. Ironically, these probes are among those that most require correction because they yield EPR spectra that remain unresolved even under conditions in which the intrinsic linewidth comprises as little as 15% of the observed linewidth. The purpose of the present work is to determine the hyperfine structure from the NMR and EPR spectra of a series of doxyl-labeled *n*-alkyl chains. In the literature, the structures of doxylpropane and doxylcyclohexane have been deduced from NMR (7, 12) and doxylcyclododecane has been studied by ENDOR (13). Our aim in commencing this work was to measure the hyperfine coupling constants large enough to materially affect the EPR correction procedures, but the 500 MHz NMR spectra were so stunningly resolved and revealed some interesting magnetically inequivalencies that we have made an effort to interpret the data comprehensively.

Figure 1 gives the structures of the spin probes studied, the labeling conventions used, and the structure and names of other spin probes discussed in this paper. Ring methyl, ring methylene, and terminal chain methyl protons are denoted by  $(\text{CH}_3)_R$ ,  $(\text{CH}_2)_R$ , and  $(\text{CH}_3)_T$ , respectively. Resolved NMR lines are observed due to hyperfine coupling between the unpaired electron and protons on chain methylene groups as far as three carbon-carbon bonds away from the attachment point of the doxyl group. We number the methylene groups according to their distance from the attachment point and use primes to denote the methylene groups toward the shorter end of the molecule. In principle, for a given stereoisomer, all four protons on methylene groups  $i$  and  $i'$ ,  $i = 1-3$ , are inequivalent magnetically; thus we label the two protons on a given methylene group differently. For example,  $H_{Li}$  and  $H_{Si}$  distinguish the two protons on methylene group  $i$  by the subscripts L and S, which refer to protons having the "larger" and "smaller" hyperfine coupling, respectively. For the JN14 series, we find below that the end-to-end inequivalence is unresolved in every case except one. We use the designation "equivalent" to mean that the NMR resonances are not resolved; thus  $H_{Li}$  is equivalent to  $H_{Li'}$  and  $H_{Si}$  is equivalent to  $H_{Si'}$ ,  $i = 1-3$  and  $i' = 1'-3'$ , in every case except one. We refer to methylene or ter-

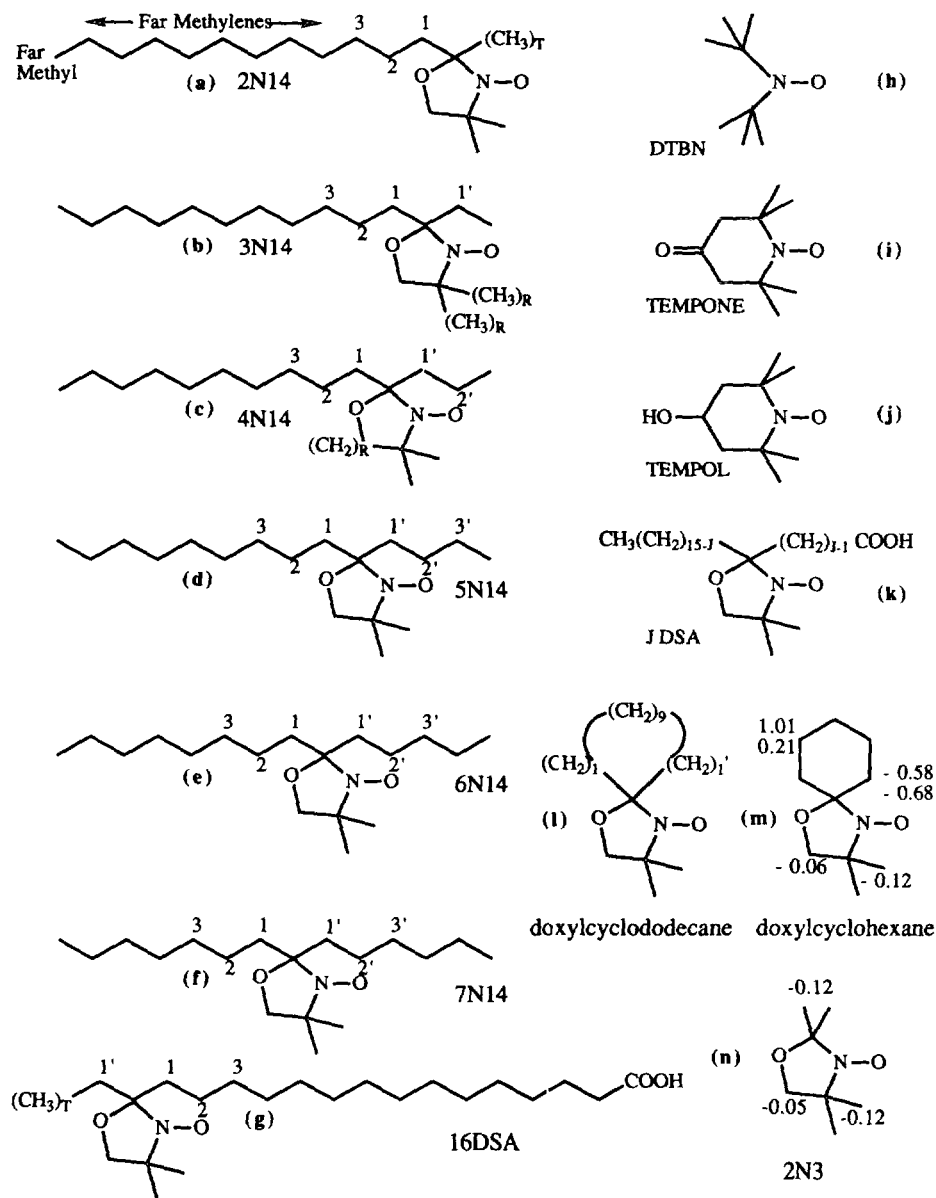


FIG. 1. (a-g) Nitroxide spin probes studied in this work. Notations for the terminal methyl, ring methyl, and ring methylene group are indicated in (a)-(c). Chain methylene groups are numbered sequentially from the doxyl attachment point employing primes to indicate those groups residing in the shorter chain. Spin probes from the literature and their trivial names are displayed in (h)-(k). Proton hyperfine coupling constants, in gauss, from the literature are indicated in (m) and (n).

minimal methyl protons farther than 3 bonds from the attachment point as being "far." There are 6 far methyl protons for  $N = 5-7$ , 3 far methyl protons for  $N = 2-4$ , and none for 16DSA. The number of far methylene protons varies as follows: 10 for  $N = 5-7$ ; 12 for 4N14; 14 for 3N14; 16 for 2N14; and 22 for 16DSA.

### THEORY

#### NMR

NMR spectra of free radicals can give the magnitude and sign of the hyperfine coupling constants from paramagnetic

shifts under conditions of fast electron spin exchange (2, 4, 5, 8). The coupling constant with the  $j$ th proton may be computed from the paramagnetic shifts by

$$a_j = -\Delta H_j / [(\gamma_e / \gamma_N)(g\beta H / 4kT)], \quad [1]$$

where the paramagnetic shift  $\Delta H_j$  is the shift in resonance field of the proton due to hyperfine interaction of the proton with the unpaired electron. The other symbols are standard (2, 4, 5, 8). The shift  $\Delta H_j$  is taken to be the difference in resonance fields of a proton in the nitroxide free radical and

the corresponding amine. Equation [1], with  $a_j$  in gauss, may be rewritten at 500 MHz as

$$a_j = 4.50 \times 10^{-5} T (\delta_{\text{para}} - \delta_{\text{dia}}), \quad [2]$$

where  $\delta_{\text{para}}$  and  $\delta_{\text{dia}}$  are the frequency shifts (ppm) in the nitroxide and the corresponding amine, respectively. All frequency shifts in this paper are given relative to TMS.

### EPR

If the hyperfine structure due to the protons is unresolved, EPR spectra of nitroxide spin probes reorienting in the fast-motion regime are the envelopes of overlapping lines of intrinsic width,  $\Delta H_{\text{pp}}^{\text{L}}$ , in most cases adequately assumed to be the same for all the lines ( $I$ ). The complexity of the hyperfine structure varies from simple 13-line patterns of binomial relative intensity for TEMPONE to very complicated patterns of more than 2000 lines for TEMPOL ( $I$ ), and yet almost all of the envelopes produced by these patterns are quite accurately represented by a Gaussian-Lorentzian convolution, the so-called Voigt lineshape. The only known exceptions are those patterns in which the hyperfine coupling to a single proton is much larger than the hyperfine couplings to all of the other protons ( $II$ ). The square of the Gaussian linewidth is given by ( $I$ )

$$(\Delta H_{\text{pp}}^{\text{G}})^2 = \alpha \sum N_j (a_j)^2, \quad [3]$$

where  $a_j$  is the hyperfine coupling constant of the  $j$ th set of  $N_j$  equivalent protons and  $\alpha$  is a factor, near unity, that, in theory, takes into account the difference in binomial patterns and Gaussian envelopes. In practice,  $\alpha$  is adjusted to optimize the precision of the Dobryakov-Lebedev relation between  $\Delta H_{\text{pp}}^{\text{G}}$  and  $\Delta H_{\text{pp}}^{\text{L}}$  ( $14$ ),

$$\left( \frac{\Delta H_{\text{pp}}^{\text{G}}}{\Delta H_{\text{pp}}^{\text{L}}} \right)^2 + \frac{\Delta H_{\text{pp}}^{\text{L}}}{\Delta H_{\text{pp}}^{\text{G}}} = 1, \quad [4]$$

where  $\Delta H_{\text{pp}}^{\text{L}}$  is the linewidth of the envelope. Equation [4] is valid for first-derivative spectra; this paper deals only with such spectra. The degree of inhomogeneous broadening is given quantitatively by the value of the Voigt parameter,

$$\chi \equiv \frac{\Delta H_{\text{pp}}^{\text{G}}}{\Delta H_{\text{pp}}^{\text{L}}}. \quad [5]$$

All of the correction procedures were formulated ( $I$ ) in terms of  $\chi$  and were found to be universal up to  $\chi \approx 2$  with precision sufficient for most work; that is, all spin labels are corrected with the same equations. For spin labels in which the hyperfine structure is unknown, and  $\Delta H_{\text{pp}}^{\text{G}}$  is therefore unavailable from Eq. [3], a procedure was developed to estimate  $\chi$  from measurements of a lineshape parameter,  $\psi$ ,

found by measuring the intensity of the EPR spectrum in the wings of the lines. The parameter  $\psi$  is related to  $\chi$  by the empirical equation ( $I$ )

$$\chi_{\text{universal}} = \frac{-0.7624\psi^2 + 0.4091\psi - 0.0527}{\psi^2 - 0.2591\psi + 0.0075}. \quad [6]$$

The subscript *universal* refers to a fictitious hyperfine pattern designed to remain unresolved at large values of  $\chi$  and has been used heretofore ( $I$ ) to correct EPR of the doxyl-labeled alkyl chains. The universal pattern was found to be more accurate than the Voigt-shape in the correction procedures ( $I$ ). A value of  $\alpha^{1/2} = 1.07$  was used to derive Eq. [6] ( $I$ ). Our intention was to replace Eq. [6] with an empirical equation derived from the present work, but Eq. [6] has proved to be quite precise, so we have decided to leave it intact.

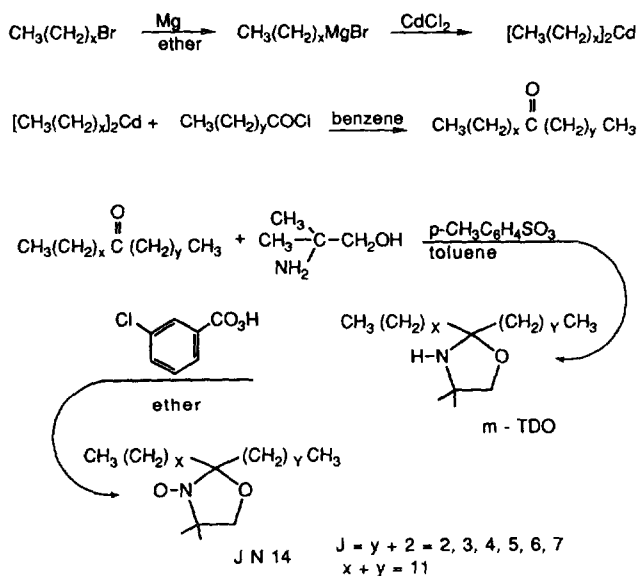
## MATERIALS AND METHODS

### NMR

NMR spectra were measured at 500 MHz at the CalTech NMR regional facility, sponsored by the NSF (Grant CHE 84-40137). Impurity peaks of  $\text{CD}_2\text{HOD}$ ,  $\delta$  3.3, and  $\text{C}_6\text{D}_5\text{H}$ ,  $\delta$  7.15, relative to TMS served as internal standards in most cases. Some samples containing TMS were run as checks. The  $\delta_{\text{dia}}$  were measured in the corresponding amines in  $\text{C}_6\text{D}_6$  as follows: for  $J = 3-7$  in  $\text{C}_6\text{D}_6$  and  $J = 7$  in  $\text{CD}_3\text{OD}$ ,  $(\text{CH}_2)_{\text{R}}$ ,  $\delta$  3.50;  $(\text{CH}_3)_{\text{R}}$ ,  $\delta$  1.08;  $(\text{CH}_3)_{\text{T}}$ ,  $\delta$  0.86;  $(\text{CH}_2)_{\text{1}}$ ,  $\delta$  1.46;  $(\text{CH}_2)_{\text{2}}$ ,  $\delta$  1.24; and  $(\text{CH}_2)_{\text{3}}$ ,  $\delta$  1.24. For  $J = 2$  in  $\text{C}_6\text{D}_6$ , the diamagnetic shifts were the same except for  $(\text{CH}_2)_{\text{R}}$ ,  $\delta$  3.45. For 16DSA in  $\text{CCl}_3\text{D}$ , the diamagnetic shifts were the same except for  $(\text{CH}_3)_{\text{R}}$ ,  $\delta$  1.22. The errors quoted in Table 4 include the errors involved in neglecting the solvent and temperature dependence of  $\delta_{\text{dia}}$  and in most cases are minor compared with uncertainties in  $\delta_{\text{para}}$ . 16DSA was purchased from Molecular Probes and used as received; 1.7  $M$  solutions of JN14 and 16DSA were prepared in deuterated solvents obtained from Aldrich and used as received. Thin-bore NMR tubes were used to conserve material. NMR samples were not degassed. The temperature was calibrated using the known variation of methanol resonances and controlled with a Bruker variable-temperature apparatus.

### EPR

EPR spectra were obtained on a Bruker spectrometer operating at 9.55 GHz. The temperature was controlled to  $298 \pm 0.1^\circ\text{C}$  by passing thermostated odorless kerosene through a homemade double-walled quartz Dewar inside the microwave cavity. The spectrometer was controlled, and spectra were digitized and stored on floppy disks, by an IBM 9000 workstation. The spectra were transferred to a PC clone and analyzed using a nonlinear least-squares fitting procedure,



SCHEME 1

written in the language C, similar to that recently described (15). The procedure takes advantage of the fact that the Voigt shape is approximated to excellent precision by a sum of Gaussian and Lorentzian functions given by Eq. [13] of Ref. (1).

EPR samples,  $6 \times 10^{-4} M$ , were prepared by dissolving the free radical in 99+% spectrophotometric-grade toluene which was used as received. The solutions were degassed by bubbling dry nitrogen gas for a few minutes and were sealed into 50  $\mu\text{l}$  disposable pipettes which were placed into the thermostated dewar for measurement. Small amounts of dissolved oxygen do not affect the Gaussian linewidth (1).

### Synthesis

**Tetradecanones.** Each of the six isomeric straight-chain tetradecanones was prepared by formation of the organo-cadmium reagent (16, 17) from the *n*-alkyl bromide corresponding to the longer end of the molecule for subsequent reaction with the acid chloride corresponding to the shorter end (see Scheme 1). These ketones were distilled at reduced pressure with considerable difficulty (vigorous frothing); the boiling ranges proved to be quite wide. Foreruns were rejected and substantial residues remained. Boiling points were generally approximately  $150^\circ\text{C}/15 \text{ mm}$ . Infrared and mass spectral data are presented in Table 1.

The acid chlorides were prepared by reaction of the appropriate carboxylic acid with thionyl chloride. Undecyl bromide was prepared by a modified Hunsdiecker reaction (18) beginning with lauric acid.

As a typical example, magnesium (2.43 g, 0.10 mol) was suspended in anhydrous diethyl ether (40 ml) and 1-bro-

TABLE 1  
Infrared and Mass Spectral Data

Compound	IR ( $\text{cm}^{-1}$ ) <sup>a</sup>	Mass spectrum ( <i>m/z</i> )
2-Tetradecanone <sup>b</sup> (2-TDO)	1721 3350vw, 1370, 1160w, 1047	— 283 ( $M^+$ , w), 282, 268, 114 (base)
3-Tetradecanone <sup>c</sup> (3-TDO)	1721 3350vw, 1192, 1053	— 283 ( $M^+$ , w), 282, 254, 128 (base)
4-Tetradecanone <sup>d,e</sup> (4-TDO)	1718 3350vw, 1190, 1055	212 ( $M^+$ ), 169, 43 (base) 283 ( $M^+$ , w), 282, 240 (base)
5-Tetradecanone <sup>d</sup> (5-TDO)	1719 3350vw, 1185, 1050	212 ( $M^+$ ), 155, 57 (base), 43 283 ( $M^+$ , w), 282, 254, 226 (base)
6-Tetradecanone <sup>d</sup> (6-TDO)	1722 3350vw, 1200w, 1160, 1045	212 ( $M^+$ ), 141, 57, 43 (base) 283 ( $M^+$ , w), 282, 212, 170 (base)
7-Tetradecanone <sup>d</sup> (7-TDO)	1720 3360vw, 1190, 1160w, 1055	212 ( $M^+$ ), 127, 57, 43 (base) 283 ( $M^+$ , w), 282, 198 (base)

Note. *m*-Tetradecanones and 4',4'-dimethylloxazolidine derivatives of *m*-tetradecanones (*m*-TDO).

<sup>a</sup> Film.

<sup>b</sup> Available from Lachat Chemicals, Inc., Chicago Heights, Illinois.

<sup>c</sup> Available from Calbiochem, Los Angeles, California.

<sup>d</sup> From Ref. (30).

<sup>e</sup> Semicarbazone mp  $34\text{--}36^\circ\text{C}$  (aq. alcohol).

mooctane (19.3 g, 0.10 mol) in anhydrous ether (125 ml) was added dropwise with mechanical stirring. The mixture was then heated at reflux until nearly all the magnesium had reacted. The flask was then chilled in ice and powdered, anhydrous cadmium chloride (9.51 g, 0.52 mol) was added at once with stirring. The ice bath was removed, the mixture was stirred for a half-hour, and the solvent was removed by distillation. Anhydrous benzene (125 ml) was added, followed by a solution of caproyl chloride (10.2 g, 0.076 mol) in benzene (40 ml) over about 10 minutes with rapid mechanical stirring. The mixture was heated at reflux for one hour and then cooled in ice. Water (50 ml) was added slowly, followed by a large excess of 0.1 M H<sub>2</sub>SO<sub>4</sub> to form two distinct layers. The benzene layer was separated, washed with sat. aq. NaHCO<sub>3</sub> and water, and dried over Na<sub>2</sub>SO<sub>4</sub>. Solvent was removed at reduced pressure to leave 13.6 g of light yellow oil which was distilled (with considerable difficulty because of frothing). A fraction boiling at about 160–173°C/45 mm was collected to provide 6-tetradecanone as a colorless oil (8.5 g).

*4',4'-Dimethyloxazolidine derivatives of m-tetradecanones (m-TDO).* The tetradecanones were converted to the 4',4'-dimethyloxazolidine derivatives (*m*-TDO) by the method of Keana *et al.* (19). The products were not purified at this stage, but oxidized directly to the N-oxyl compounds.

As a typical example, a mixture of 6-tetradecanone (6.0 g, 0.027 mol), 2-amino-2-methyl-1-propanol (28 ml, 0.27 mol), *p*-toluenesulfonic acid monohydrate (about 100 mg), and toluene (200 ml) was heated at reflux for six days using a Dean–Stark apparatus for water removal. The solution was washed with sat. aq. NaHCO<sub>3</sub> (2 × 100 ml) and with water (3 × 100 ml) and dried over Na<sub>2</sub>SO<sub>4</sub>. Solvent was removed at reduced pressure to leave the 4',4'-dimethyloxazolidine derivative of 6-tetradecanone (6-TDO) as a colorless oil (7.3 g).

*N-Oxyl-4',4'-dimethyloxazolidine derivatives of m-tetradecanones (m-TDNO).* The oxazolidines were oxidized with *m*-chloroperbenzoic acid to yield the N-oxyl derivatives (17, 19), which were isolated in about 30–40% yield by chromatography on silica gel. These yellow–orange oils could be subjected to Kugelrohr distillation at 120–125°C/0.2 mm. The infrared, mass spectral, and combustion analyses of these compounds are presented in Table 2.

As a typical example, the 4',4'-dimethyloxazolidine derivative of 6-tetradecanone (4.00 g, 0.0141 mol) was dissolved in anhydrous diethyl ether (75 ml) and cooled in ice. A solution of *m*-chloroperbenzoic acid (Aldrich Chemical Co., 85%, 2.94 g, 0.0145 mol) in anhydrous ether (50 ml) was added dropwise, with stirring, over 1 hour. The reaction mixture was kept in ice for an additional 3–4 hours and then allowed to stir at room temperature for 45 hours. The solution was washed with sat. aq. NaHCO<sub>3</sub> (4 × 50 ml) and dried over Na<sub>2</sub>SO<sub>4</sub>. Solvent was removed at reduced pressure to leave a yellow oil (4.02 g). A 2.0 g sample of this material was chromatographed over about 40 g of Act.III silica gel. A 1:9 mixture of CH<sub>2</sub>Cl<sub>2</sub>:petroleum ether (30–60°C) eluted 0.62 g of the N-oxyl-4',4'-dimethyloxazolidine derivative of 6-tetradecanone (6-TDNO) as a yellow–orange oil. For combustion analysis, a sample of this oil was chromatographed on a thick-layer silica plate with 2:3 CH<sub>2</sub>Cl<sub>2</sub>:petroleum ether, followed by double Kugelrohr distillation at 120°C/0.2 mm.

## RESULTS

### NMR

Figure 2 shows the NMR spectrum of 7N14 in C<sub>6</sub>D<sub>6</sub> at 296 K. The peaks due to TMS and C<sub>6</sub>D<sub>5</sub>H ( $\delta$  7.15) are noted. Four broad peaks, which are barely discernible at this receiver gain, especially one at  $\delta$  of –24.81, are more easily observed in Fig. 3, which is displayed at a higher amplification. The

TABLE 2  
Analysis of N-Oxyl-4',4'-dimethyloxazolidine Derivatives of *m*-Tetradecanones

<i>m</i>	Combustion <sup>a</sup>	IR (cm <sup>-1</sup> )	Mass spectrum ( <i>m/z</i> )
2	C, 72.70; H, 12.04; N, 4.63	1242w, 1042	298 (M <sup>+</sup> ), 242, 213 (base) 298.2739 (M <sup>+</sup> ), <sup>b</sup> 213.2216 <sup>c</sup>
3	C, 72.73; H, 11.99; N, 4.67	1252, 1238w, 1048	298 (M <sup>+</sup> ), 242, 213 (base) 298.2748 (M <sup>+</sup> ), <sup>b</sup> 213.2209 <sup>c</sup>
4	C, 72.60; H, 12.16; N, 4.64	1253, 1240w, 1048	298 (M <sup>+</sup> ), 242, 213 (base)
5	C, 72.62; H, 12.14; N, 4.46	1255, 1240w, 1044	298 (M <sup>+</sup> ), 242, 214, 213 (base)
6	C, 72.51; H, 12.26; N, 4.74	1250, 1240w, 1046	298 (M <sup>+</sup> ), 242, 213 (base)
7	C, 72.70; H, 12.07; N, 4.81	1255, 1238w, 1049	298 (M <sup>+</sup> ), 242, 214, 213 (base)

<sup>a</sup> Combustion analyses performed by P. Borda, Department of Chemistry, University of British Columbia. Cald for C<sub>18</sub>H<sub>36</sub>NO<sub>2</sub>: C, 72.43; H, 12.16; N, 4.69.

<sup>b</sup> High resolution. Cald for C<sub>18</sub>H<sub>36</sub>NO<sub>2</sub>: 298.2746.

<sup>c</sup> High resolution. Cald for C<sub>14</sub>H<sub>20</sub>O: 213.2219.

TABLE 3  
Integrated Intensities of NMR Lines<sup>a</sup>

	(CH <sub>3</sub> ) <sub>R</sub>	H <sub>L1</sub> + H <sub>L1'</sub>	H <sub>S1</sub> + H <sub>S1'</sub>	H <sub>S2</sub> + H <sub>S2'</sub> + H <sub>L2</sub> + H <sub>L2'</sub>	H <sub>S3</sub> + H <sub>S3'</sub> + H <sub>L3</sub> + H <sub>L3'</sub>	(CH <sub>3</sub> ) <sub>T</sub>
2N14	6.0/6	0.7 ± 0.3/1	1.2 ± 0.3/1	1.5/2		3.2/3
3N14	5.5/6	1.6/2	2.0/2	1.7/2	2.0/2	2.8/3
4N14	6.3/6	2.0/2	2.0/2	4.3/4	2.4/2	2.9/3
5N14	6.0/6	1.7/2	1.9/2	4.0/4	4.1/4	
6N14	5.9/6	1.9/2	2.0/2	4.2/4	4.6/4	
7N14	6.2/6	2.0/2	2.0/2	4.2/4	5.3/4	
16DSA	6.1/6	1.6/2	2.0/2	2.9/2		3.3/3

<sup>a</sup> Except for those explicitly noted, the errors are estimated at 5% for (CH<sub>3</sub>)<sub>R</sub> and H<sub>L1</sub>, H<sub>S1</sub>; 10% for the (CH<sub>3</sub>)<sub>T</sub>, and 15% for the others. Theoretically expected intensities based upon the assignments in the text are given by the denominators.

center portion of the spectrum in Fig. 2 consists of three relatively narrow peaks at  $\delta$  0.94,  $\delta$  1.35, and  $\delta$  1.40. The peak at  $\delta$  0.94, due to the terminal methyl protons, is only slightly shifted from the resonance position in the amine,  $\delta$  0.86; therefore, according to Eq. [2], these protons have a

hyperfine interaction with the unpaired electron of less than 1 mG. The peak  $\delta$  1.35 is assigned to the far methylene protons. This shift from  $\delta$  1.24 for these protons in the corresponding amine yields hyperfine couplings of less than 1 mG. The  $\delta$  1.40 resonance is assigned to the ring methylene

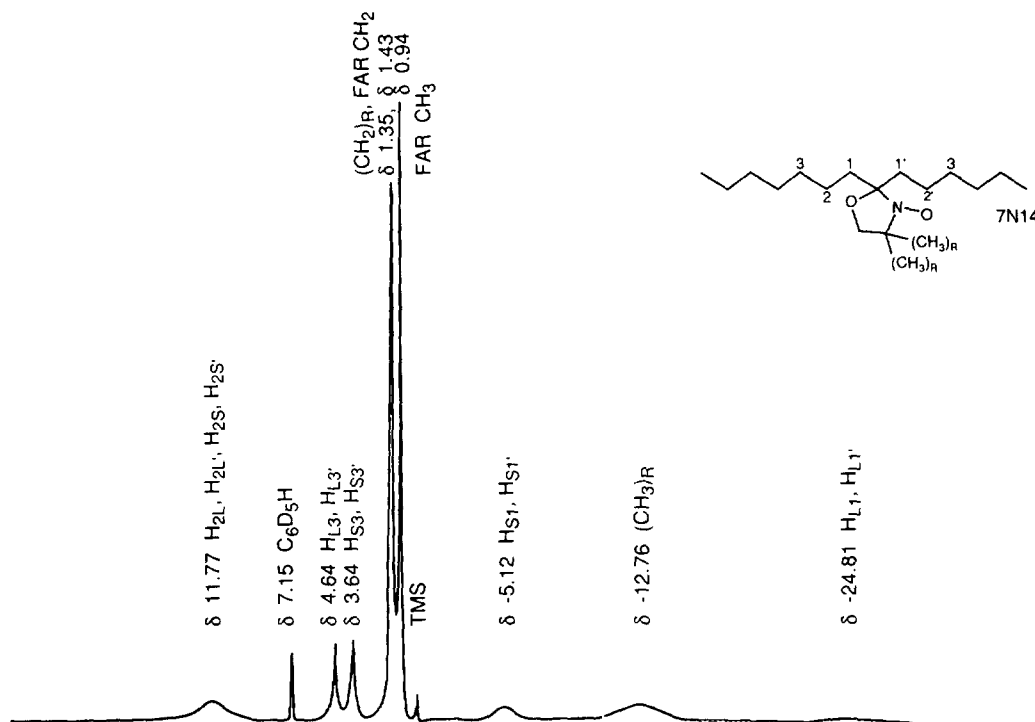


FIG. 2. NMR spectrum of 1.7 M 7N14 in C<sub>6</sub>D<sub>6</sub> at 500 MHz and 296 K. Shifts relative to TMS in ppm are indicated. Note the sharp lines due to C<sub>6</sub>D<sub>5</sub>H and TMS. The central part of the spectrum consists of a sharp line at  $\delta$  0.94 assigned to far methyl proton resonance and a pair of lines at  $\delta$  1.35 and  $\delta$  1.43 assigned to ring and far methylene protons, respectively. The doublet at  $\delta$  4.64 and  $\delta$  3.64 appears near these same frequencies for all JN14, J = 2-7, and 16DSA. Four broad lines, barely visible in this spectrum, are labeled by shift and assignment.

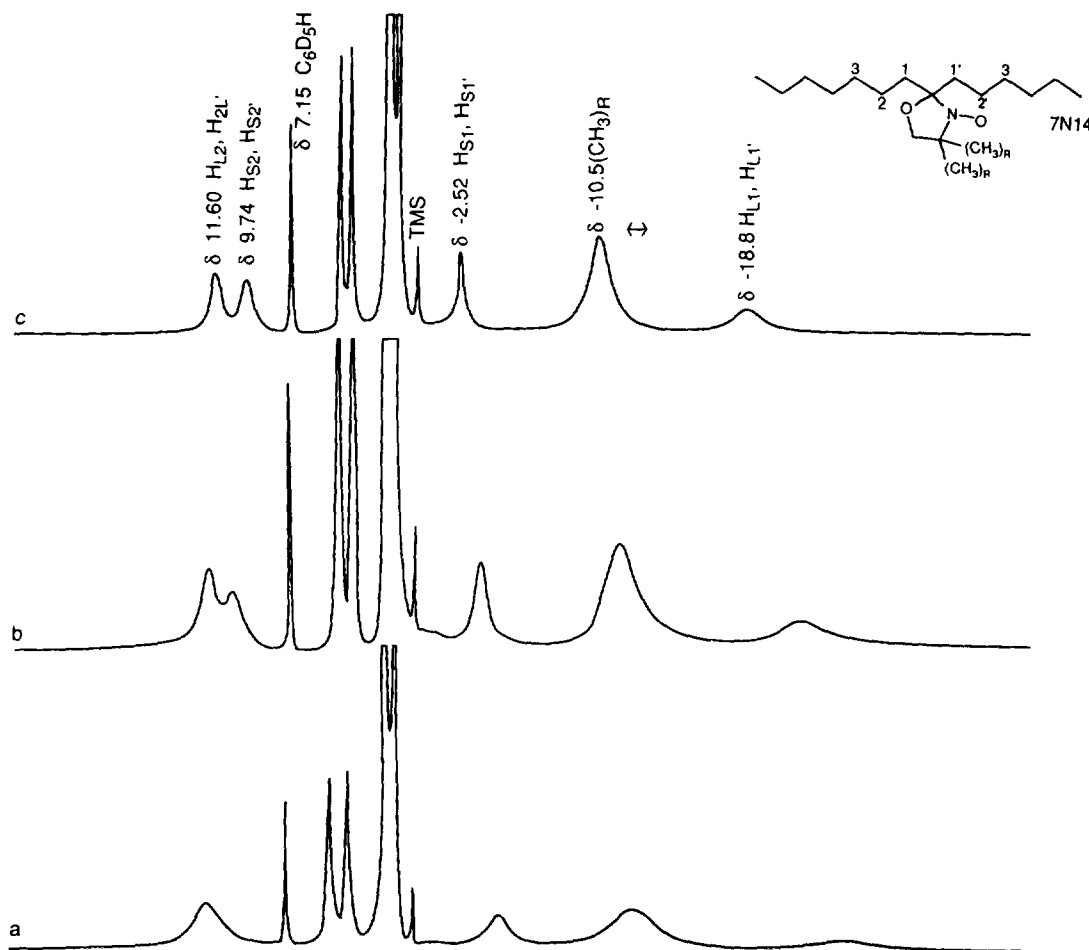


FIG. 3. NMR spectra of 1.7 *M* 7N14 in  $C_6D_6$  at 500 MHz at (a) 296 K, (b) 323 K, and (c) 353 K at higher amplification than in Fig. 2 showing broad lines. Shifts relative to TMS in ppm are indicated. The lines shift and narrow at higher temperatures. The line assigned to chain methylene protons at positions 2, 2', unresolved at 296 K, becomes resolved at higher temperatures,  $\delta$  11.60 and  $\delta$  9.74. The horizontal arrow near the  $(CH_3)_R$  resonance indicates the uncertainty in line position that would correspond to a  $\pm 10$  mG error in the hyperfine coupling constants.

protons,  $(CH_2)_R$ . Three peaks near these same resonance frequencies are observed in all six members of the series *JN*14 although they are not resolved at 296 K in all cases. Accurate integration of the overlapping central lines is not possible, but the relative heights of the peaks assigned to  $(CH_2)_R$  and far methylene protons are consistent with these assignments in those cases in which they are resolved. For example, see Fig. 4a. If the assignments of  $(CH_2)_R$  and the far methylene protons were interchanged, an error of less than 1.0 mG would be introduced into the calculation of the hyperfine coupling constants.

We now turn to the assignment of the broader peaks. Paramagnetic shifts have been rigorously assigned in the case of doxycyclohexane (Fig. 1m) (6, 7), by utilizing isotopic and chemical substitution. Using doxycyclohexane as a guide, the peak at  $\delta$  of  $-12.76$  in Fig. 2 is assigned to the ring methyl protons,  $(CH_3)_R$ . The relative intensities of the lines were determined by integration, in the normal way for

relatively narrow lines and by two other approaches for broader lines as follows: (i) the full width at half-height was multiplied by the height and (ii) the profile of the line was cut from paper and weighed several times, both with and without an effort to follow the sloping baseline. Averaging the results of these approaches yields uncertainties of about 5% for  $(CH_3)_R$  and the line shortly to be assigned to the overlapping resonances of  $H_{S1}$  and  $H_{S1'}$ . The more reproducible of these two intensities was set equal to 6.0 or 2.0, respectively, in Table 3, where the relative intensities are presented. The intensity of the  $(CH_3)_T$  was reproducible to about 10%, and the others, except for 2N14, are uncertain by about 15%.

The pair of peaks at  $\delta$  4.64 and  $\delta$  3.64 in Fig. 2 appears in the NMR spectra of all *JN*14 and 16DSA at almost precisely the same frequencies. The integrated intensity of these two peaks is near 4 for 7N14, 6N14, and 5N14 and drops to near 2 for 4N14 and 3N14. This is the pattern expected

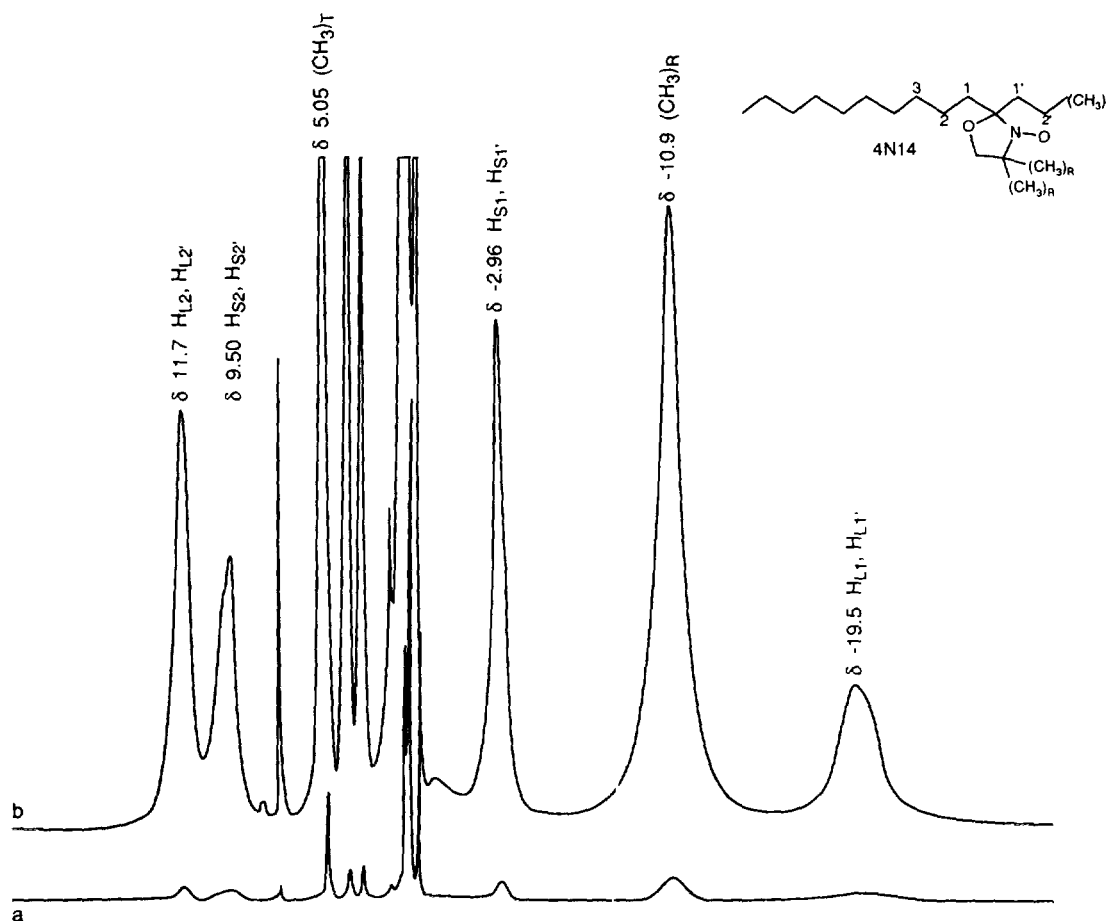


FIG. 4. NMR spectra of 1.7 *M* 4N14 in  $C_6D_6$  at 500 MHz at 353 K at low (a) and higher (b) gain. The terminal methyl proton resonance appears at  $\delta$  5.05. The rest of the lines are very similar to those in Figs. 2 and 3, including the pair at  $\delta$  11.75 and  $\delta$  9.50, except this latter line shows some asymmetry, perhaps signaling the onset of end-to-end inequivalence in the 2, 2' positions.

for the protons on methylene carbons 3 and 3' and is thus assigned. It is immediately evident that the small inequivalency between the  $\delta$  4.64 and  $\delta$  3.64 resonances is not due to an inequivalency between positions 3 and 3' because this difference persists for 4N14 and 3N14, which do not have 3' positions. It is also immediately evident that the spin density distribution of the unpaired electron three carbons removed from the doxyl attachment point is insensitive to the position of the attachment even if it is near the end of the chain.

The line at  $\delta$  11.77 in Fig. 2 has a relative intensity near 4 for 7N14,  $J = 4-7$ , and drops to near 2 for  $J = 2-3$ . This resonance is assigned to the protons on the 2 and 2' methylene carbons using the same reasoning as that in the previous paragraph. The peak at  $\delta$  of  $-24.8$  is assigned to protons at positions 1, 1' based on the fact that the hyperfine couplings at the comparable positions in doxylcyclohexane are large and negative. These resonances integrate to only near 2, falling to near 1 or less for 2N14, showing that only two of the four protons on methylene carbons 1, 1' resonate at this

frequency. EPR spectra are also inconsistent with four large hyperfine coupling constants. The remaining peak at  $\delta$  of  $-5.12$  is assigned to the other two 1, 1' protons. The hyperfine coupling constants computed from Eq. [2] are given in Table 4. Conceivably, the assignment of 1, 1' protons and the ring methylene protons could be interchanged, but we favor the present assignment for two reasons: first, the coupling constant observed here for  $(CH_2)_R$ ,  $\approx -0.03$  G, compares better with the result in doxylpropane,  $-0.05$  G, and doxylcyclohexane,  $-0.06$  G, than it would if the assignments were switched,  $-0.115$  G. Second, the temperature and solvent dependence of the  $H_{L1}$  and  $H_{S1}$  coupling constants, as assigned, are well correlated. The temperature variations of  $(CH_2)_R$  and  $(CH_3)_R$  coupling constants are both small with the proposed assignment. For the purpose of correcting EPR spectra, the difference is immaterial.

The NMR spectrum of 7N14 in  $C_6D_6$  at higher amplification is given in Fig. 3a at 296 K. The four broad lines are shown in Fig. 3b at 323 K and Fig. 3c at 353 K. All of the lines are seen to narrow with increasing temperature, due to



TABLE 4  
Hyperfine Coupling Constants (mG) Derived from NMR Paramagnetic Shifts<sup>a</sup>

Probe Solvent	<i>T</i> (±1 K)	(CH <sub>3</sub> ) <sub>R</sub>	(CH <sub>2</sub> ) <sub>R</sub> (±1 mG)	(CH <sub>3</sub> ) <sub>T</sub>	Next three columns	1, 1'	2, 2'	3, 3' (±1 mG)
2N14	296	-157 (5)	-29	-53 (3)	H <sub>L</sub>	—	113 (3) <sup>c,e</sup>	68 <sup>d</sup>
					H <sub>S</sub>	-137 (8) <sup>b</sup>		46 <sup>d</sup>
C <sub>6</sub> D <sub>6</sub>	323	-161 (3)	-32	-65 (2)	H <sub>L</sub>	-360 (14) <sup>b</sup>	124 (3) <sup>c,e</sup>	68 <sup>d</sup>
					H <sub>S</sub>	-117 (2) <sup>b</sup>		50 <sup>d</sup>
	353	-168 (2)	-32	-73 (2)	H <sub>L</sub>	-365 (7) <sup>b</sup>	135 (3) <sup>c</sup>	66 <sup>d</sup>
					H <sub>S</sub>	-104 (5) <sup>b</sup>	122 (8) <sup>c</sup>	55 <sup>d</sup>
3N14	296	-185 (2)	-30	238 (2)	H <sub>L</sub>	-351 (4), -327 (3)	140 (+3, -6) <sup>c,e</sup>	43 <sup>d</sup>
					H <sub>S</sub>	-89 (2)		30 <sup>d</sup>
C <sub>6</sub> D <sub>6</sub>	323	-187 (2)	-33	240 (2)	H <sub>L</sub>	-342 (3), -316 (3)	154 (3) <sup>c</sup>	43 <sup>d</sup>
					H <sub>S</sub>	-80 (2)	134 (3) <sup>c</sup>	33 <sup>d</sup>
	353	-190 (2)	-34	246 (2)	H <sub>L</sub>	-341 (3), -312 (4)	166 (2) <sup>c</sup>	43 <sup>d</sup>
					H <sub>S</sub>	-70	138 (2) <sup>c</sup>	33 <sup>d</sup>
4N14	296	-184 (2)	-30	72 (1)	H <sub>L</sub>	-351 (-3, +5)	142 (2)	44 <sup>d</sup>
					H <sub>S</sub>	-86 (2)	127 (4)	32 <sup>d</sup>
C <sub>6</sub> D <sub>6</sub>	323	-187 (2)	-32	69 (1)	H <sub>L</sub>	-339 (-3, +5)	154 (2)	44 <sup>d</sup>
					H <sub>S</sub>	-78 (2)	126 (4)	32 <sup>d</sup>
	353	-190 (2)	-34	67 (1)	H <sub>L</sub>	-333 (-3, +4)	166 (2)	45 <sup>d</sup>
					H <sub>S</sub>	-70 (2)	131 (4)	34 <sup>d</sup>
5N14	296	-184 (2)	-30		H <sub>L</sub>	-348 (4)	140 (+3, -5) <sup>c,e</sup>	45
					H <sub>S</sub>	-85 (2)		32
C <sub>6</sub> D <sub>6</sub>	323	-186 (2)	-33		H <sub>L</sub>	-343 (4)	152 (2)	45
					H <sub>S</sub>	-77 (2)	134 (4)	33
	353	-190 (2)	-33		H <sub>L</sub>	-339 (3)	165 (2)	45
					H <sub>S</sub>	-70 (2)	136 (3)	35
6N14	296	-186 (2)	-29		H <sub>L</sub>	-350 (3)	140 (+3, -5) <sup>c,e</sup>	45
					H <sub>S</sub>	-86 (2)		31
C <sub>6</sub> D <sub>6</sub>	323	-187 (2)	-32		H <sub>L</sub>	-344 (3)	153 (2)	44
					H <sub>S</sub>	-78 (2)	134 (4)	32
	353	-191 (2)	-33		H <sub>L</sub>	-339 (3)	165 (2)	45
					H <sub>S</sub>	-70 (2)	137 (2)	34
7N14	296	-185 (2)	-29		H <sub>L</sub>	-350 (3)	140 (+3, -5) <sup>c,e</sup>	45
					H <sub>S</sub>	-85 (2)		32
C <sub>6</sub> D <sub>6</sub>	323	-185 (2)	-32		H <sub>L</sub>	-338 (3)	154 (2)	44
					H <sub>S</sub>	-75 (2)	134 (4)	33
	353	-184 (2)	-33		H <sub>L</sub>	-322 (3)	165 (2)	43
					H <sub>S</sub>	-63 (2)	135 (2)	33
7N14	297	-175 (2)	-30		H <sub>L</sub>	-359 (3)	140 (+3, -5) <sup>c,e</sup>	48
					H <sub>S</sub>	-103 (2)		35
CD <sub>3</sub> OD	323	-176 (2)	-32		H <sub>L</sub>	-349 (3)	153 (2)	48
					H <sub>S</sub>	-94 (2)	134 (4)	36
16DSA	307	-171 (2)	-30	237 (2)	H <sub>L</sub>	-309 (9)	138 (6) <sup>c</sup>	47 <sup>d</sup>
					H <sub>S</sub>	-87 (2)	118 (8) <sup>c</sup>	33 <sup>d</sup>
CCl <sub>3</sub> D	323	-174 (2)	-32	239 (2)	H <sub>L</sub>	-340 (7), -307 (5)	148 (5) <sup>c</sup>	46 <sup>d</sup>
					H <sub>S</sub>	-81 (2)	109 (7) <sup>c</sup>	34 <sup>d</sup>

<sup>a</sup> In all cases except 3N14 and 16DSA, values quoted for positions 1, 2, and 3 are equal to those for positions 1', 2', and 3' for probes in which these latter positions exist. For 3N14 and 16DSA, the double entry under (CH<sub>2</sub>)<sub>R</sub> refers to 1 and 1'. Hyperfine couplings to inequivalent protons on the same methylene group, labeled H<sub>L</sub> and H<sub>S</sub>, are given on two lines where applicable. Uncertainties, in milligauss, are quoted at the top of the column or in parentheses and are computed as the square root of the sum of the squares of the error from uncertainty in temperature (±0.4–0.7%) and the estimated uncertainty in locating the position of the NMR line. In most cases, except for 2N14 and 16DSA, the temperature uncertainty dominates the uncertainty.

<sup>b</sup> The 1' position does not exist.

<sup>c</sup> The 2' position does not exist.

<sup>d</sup> The 3' position does not exist.

<sup>e</sup> Resonances due to H<sub>L2</sub>, H<sub>S2</sub>, H<sub>L2'</sub>, and H<sub>S2'</sub> are unresolved at this temperature.

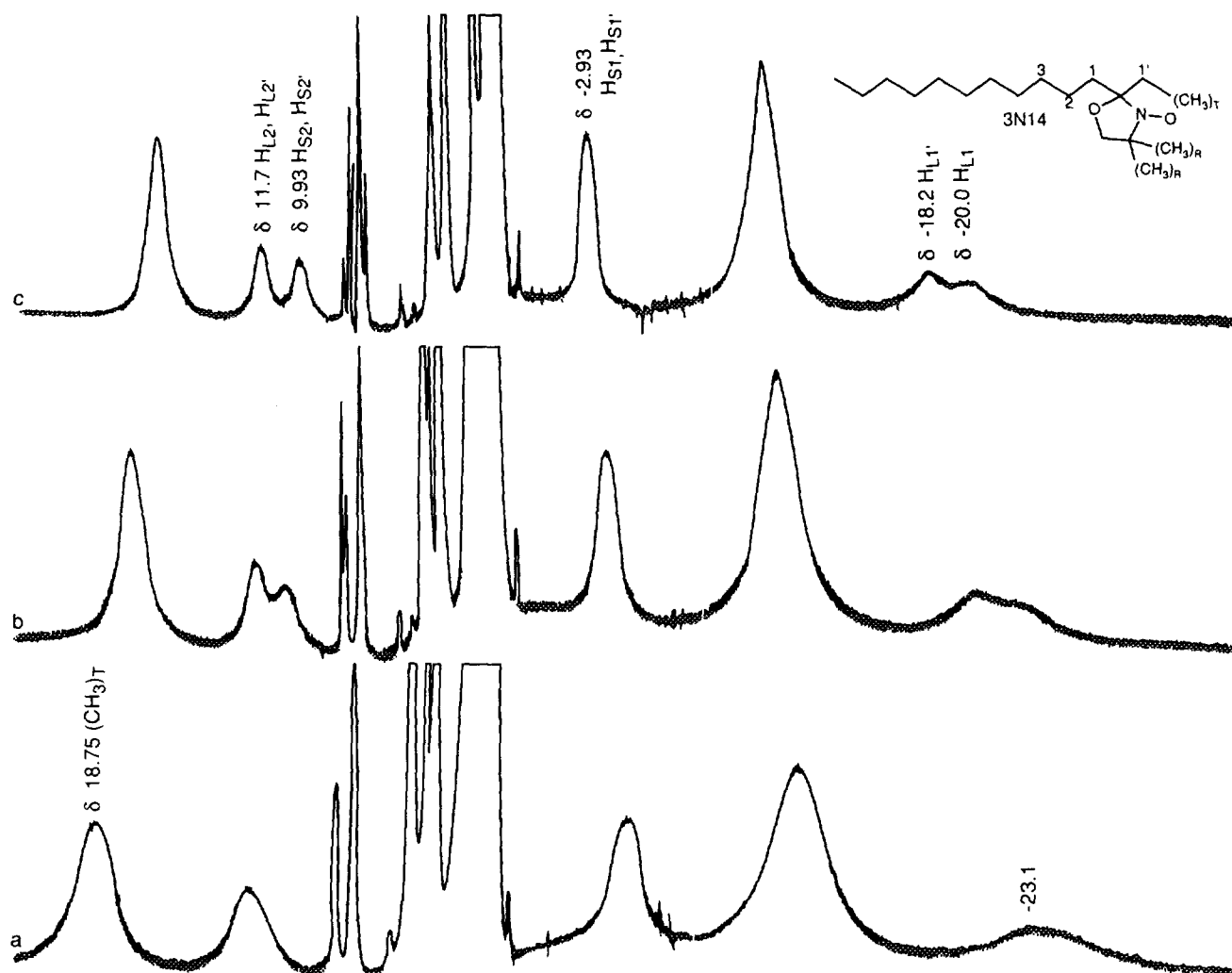


FIG. 5. NMR spectra of 1.7 *M* 3N14 in  $C_6D_6$  at 500 MHz at (a) 296 K, (b) 323 K, and (c) 353 K. The terminal methyl proton resonance now appears at  $\delta$  18.75. The rest of the lines are very similar to those in Figs. 2–4 except that the line at  $\delta$  of  $-23.1$  at 296 K (a) splits into two at  $\delta$  of  $-18.2$  and  $\delta$  of  $-20.0$  at 353 K. In 3N14, these lines correspond to the large coupling to the 1, 1' methylene protons showing the only resolved end-to-end inequivalence in hyperfine coupling constants in this study. Comparison of the two lines at  $\delta$  11.7 and  $\delta$  9.93 with Fig. 3c shows that they have nearly identical resonance frequencies but are one-half the relative intensity of those in 3N14. This shows that the inequivalency in these two lines cannot be end-to-end since 3N14 does not possess a 2' position.

increased spin exchange brought on by increased translational motion at higher  $T/\eta$ , where  $\eta$  is the shear viscosity of the solution. In addition, the formerly single line at  $\delta$  11.77 observed at 296 K splits into two ( $\delta$  11.60,  $\delta$  9.74) at 353 K. Thus, in addition to the previously noted inequivalencies 1, 1' and 3, 3', an inequivalency is revealed for positions 2, 2' at higher temperatures. The horizontal arrow near the  $(CH_3)_R$  peak indicates the extent of shift uncertainty that corresponds to  $\pm 10$  mG in the calculation of the hyperfine coupling constants.

NMR spectra of 6N14 and 5N14 are very similar to Figs. 2 and 3 and are not shown. For complete NMR spectra, see Ref. (21). The relative height of the far terminal methyl NMR falls and that of the far methylene protons increases

as the doxyl position is moved toward one end, as is expected. Figure 4a shows the NMR spectrum of 4N14 at 353 K, with a prominent resonance due to  $(CH_3)_T$  at  $\delta$  5.05, and Fig. 4b shows the same spectrum at higher gain. Figure 5a gives the broad lines in the spectrum of 3N14 at 296 K in which the  $(CH_3)_T$  resonance now appears at  $\delta$  18.75. The variation of the broad features is displayed at higher temperatures in Figs. 5b and 5c. At 353 K, a doublet is observed at  $\delta$  11.7 and  $\delta$  9.93, almost identical to the doublet observed in 7N14 (Fig. 2), but is one-half the relative integrated intensity. Since 3N14 does not have a methylene group 2', this means that the observed inequivalency corresponds to protons on the same methylene group at position 2. Therefore, it is concluded that each of the two protons residing at all three

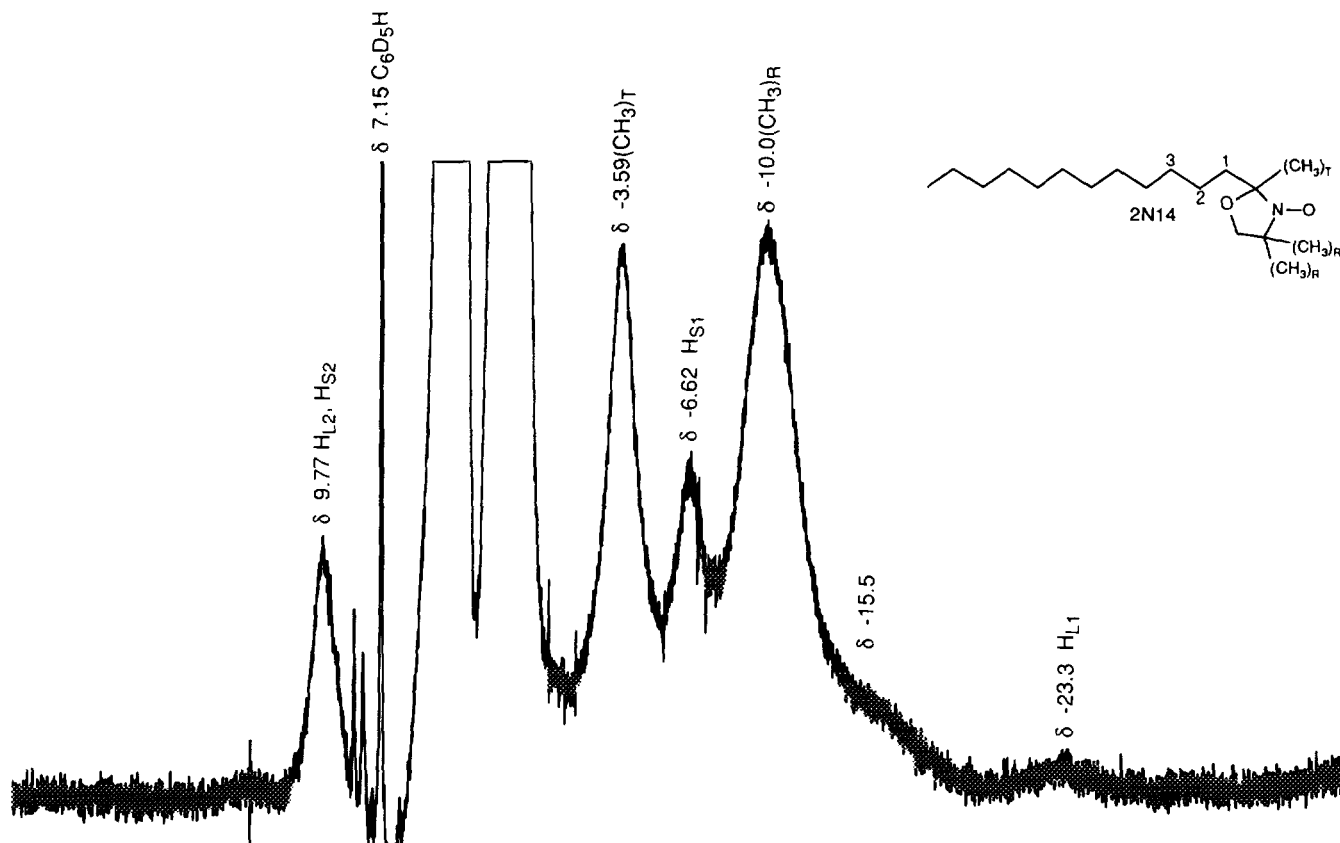


FIG. 6. NMR spectrum of 1.7 *M* 2N14 in  $C_6D_6$  at 500 MHz at 323 K. The terminal methyl proton resonance appears at  $\delta$  of  $-3.59$ . The lines are not as well resolved in this spectrum as in the other spin probes; there seems to be a broad, underlying spectrum. The resonance at  $\delta$  of  $-23.3$  is barely observable and the shoulder near  $\delta$  of  $-15.5$  might be a resonance.

methylene positions 1, 2, and 3 show inequivalent hyperfine couplings to the unpaired electron. For the lines discussed so far, it is also concluded that end-to-end inequivalencies, that is, any inequivalency between positions 1 vs 1', 2 vs 2', and 3 vs 3', is smaller than the NMR linewidths. Consider now more carefully the split resonance pair at  $\delta$  11.7 and  $\delta$  9.50 observed in 4N14 at 353 K (Fig. 4b). Although this pair is very similar to the same pair in all of the other free radicals discussed so far, including 3N14, there is an obvious asymmetry in the line at  $\delta$  9.50 giving the impression that there is an onset of a very small inequivalence between positions 2 and 2' for the protons with the smaller coupling. We find it remarkable that these two positions would be so similar given that 2' is adjacent to the terminal methyl and 2 is attached to a long alkyl chain; however, this is exactly the same result as that observed for the 3 and 3' positions. Finally, consider the pair of lines located at  $\delta$  of  $-18.2$  and  $\delta$  of  $-20.0$  at 353 K in the NMR spectrum of 3N14 (Fig. 5c). This pair, unsplit in all of the other radicals studied, shows the only unequivocal inequivalence between methylene groups symmetrically located about the attachment point of the doxyl ring. The other two protons,  $H_{S1}$  and  $H_{S1'}$ , with resonance peak at  $\delta$  of  $-2.93$ , do not show any inequiv-

alence; however, the hyperfine coupling is quite small for this pair. The NMR spectrum of 16DSA in  $CCl_3D$  is very similar to that of 3N14 in  $C_6D_6$  as is expected; however, the lines are not as narrow, perhaps because the mobility of the former is less than that of the latter, leading to less spin exchange narrowing.

Figure 6 shows the disappointing NMR spectrum of 2N14 at 323 K. A number of the lines are easy to identify, being in positions similar to those for other *J*N14, but there seems to be a broad underlying spectrum. The resonance at  $\delta$  of  $-23.3$  is barely visible; however, it is remembered that this line ought to have one-half the intensity of the same line in the other free radicals since there is no 1' position. Obviously the integration of such lines is subject to large error; nevertheless the expected drop in relative intensity of the two lines assigned to  $H_{L1}$  and  $H_{S1}$  compared with the other *J*N14 is clear. In fact, the intensity of the  $H_{L1}$  resonance seems too small (Table 3). The shoulder near  $\delta$  of  $-15.5$  might be a resonance.

Table 4 summarizes the hyperfine structure of the *J*N14 series in  $C_6D_6$  at three temperatures, of 7N14 in  $CD_3OD$  at two temperatures, and of 16DSA in  $CCl_3D$  at two temperatures. The final three columns give the couplings to chain

methylene protons and are labeled by the position of the methylene group. Since there is no difference end-to-end, except for 3N14 and 16DSA, 1 and 1', 2 and 2', and 3 and 3' are given in the same column. The double entries in the column 1, 1' for 3N14 and 16DSA correspond to the small end-to-end inequivalencies observed for those free radicals. The sixth column refers to the final free columns, denoting the smaller and larger hyperfine coupling constants observed on each chain methylene group.

## EPR

EPR spectra of JN14,  $J = 2-7$  in toluene, recorded at 298 K gave typical three-line spectra narrowed due to the rapidly rotating spin probes. Figure 7 shows the central line of 3N14 together with the simulation of the spectrum predicted by the parameters in Table 4. The algorithm of Oehler and Janzen (22) implemented on a 386 clone was used for the simulations. The only adjustable parameter used in simulating the spectrum was the intrinsic linewidth,  $\Delta H_{pp}^L$ . All other EPR spectra may be equally well simulated, including those due to 2N14. It is not possible to fit the experimental spectra for  $J = 3-7$  with a hypothesis of four large hyperfine couplings due to 1, 1' methylene protons;  $\Delta H_{pp}^G$  would be larger than  $\Delta H_{pp}^0$ . However, for 2N14, a hypothesis of two large couplings to position 1 methylene protons can yield a successful simulation.

By simulating the EPR spectra predicted by the hyperfine constants in Table 4 and varying the intrinsic linewidth,  $\Delta H_{pp}^L$ , the lineshape parameter,  $\psi$ , was obtained as described before (1). The Gaussian linewidth was calculated from the hyperfine coupling constants using Eq. [3], and Eq. [5] gave the values of  $\chi$ . The resulting curves of  $\psi$  vs  $\chi$  for JN14,  $J = 3-7$ , and 16DSA are represented by the one curve in Fig. 8 since the separate curves for each spin probe at different temperatures are not perceptibly different on the scale of Fig. 8. Also plotted in Fig. 8 is Eq. [6] demonstrating that it describes the behavior of these doxyl-labeled  $n$ -alkyl chains very well. The plot of  $\psi$  vs  $\chi$  for 2N14, using the parameters of Table 4, is not in agreement with Eq. [6]. This plot is not presented, since the NMR spectra for this spin probe seem to indicate the presence of unassigned lines that would add to the Gaussian character of the EPR lines.

As is expected (1, 15), a Gaussian/Lorentzian sum approximation of the Voigt function also yields an excellent fit to the experimental data. Rapid, automated determination of  $\Delta H_{pp}^L$  and  $\Delta H_{pp}^G$  (15) is possible for EPR spectra of spin probes such as these that are well approximated by the Voigt shape by taking advantage of the fact that a sum of a Gaussian and a Lorentzian approximates the Voigt with excellent precision (1). The advantage is that two functions are optimized rather than computing numerous lines. From the mixing parameter of the Gaussian and Lorentzian functions,  $\psi$  is

computed from Eq. [17] of Ref. (1) and  $\chi$  is given by Eq. [6]. Equations [5] and [6] yield  $\Delta H_{pp}^L$  and  $\Delta H_{pp}^G$  from  $\chi$  and measured  $\Delta H_{pp}^0$ . The results of this fitting procedure are given in Table 5 together with results calculated from the NMR data in Table 4. Both the EPR determination of  $\Delta H_{pp}^G$ , using Eq. [6] and the NMR determination, using Eq. [3] depend on the parameter  $\alpha^{1/2}$ , which has been taken to be 1.07 (1). The accuracy of  $\Delta H_{pp}^G$  is limited by the uncertainty in  $\alpha^{1/2}$ , about 5%, but the relative precision is much better than that for either EPR or NMR measurements. The standard deviations in the mean values of  $\Delta H_{pp}^G$  from EPR measurements are given in Table 5 with the number of trials indicated in parentheses. The accuracy of  $\Delta H_{pp}^G$  from the NMR measurements is dominated by the accuracy of the resonance frequencies since the temperature dependences of the hyperfine coupling constants in Eq. [3] almost cancel, yielding values of  $\Delta H_{pp}^G$  that are almost temperature independent. The solvent dependence is also small, although EPR would be a better way to study this dependence (8), because the polarity of a 1.7 M solution is probably different than the polarity of the solvent.

If we combine the NMR results at all temperatures and all JN14,  $J = 4-7$ ,  $\Delta H_{pp}^G = 0.793 \pm 0.008$  G for the 14 measurements while the mean value of the EPR measurements is  $0.800 \pm 0.010$  G. The Gaussian linewidths for these same spin probes in a different solvent were estimated previously using the four-point method (23) and compare well with the present results. A small decrease in  $\Delta H_{pp}^G$  with increasing temperature was previously interpreted (23) to be due to the onset of collapse in hyperfine structure brought on by spin exchange. Since  $\Delta H_{pp}^G$  is almost constant with temperature (Table 5), this work seems to support the earlier interpretation.

It is no surprise that the spectra due to JN14,  $J = 3-7$ , may be well simulated by a Voigt shape because the patterns fulfill the criteria for good Gaussian profiles discussed at length before (1), but the successful simulation of 2N14 is troublesome since the hyperfine pattern for 2N14 involves one large coupling constant.

## DISCUSSION

The hyperfine structure of doxyl-labeled  $n$ -alkyl chains is complex, but varies with attachment point in a very simple way. The coupling constants of  $(CH_2)_R$  and  $(CH_3)_R$  are almost identical in  $J = 3-7$  and are somewhat larger than the corresponding couplings in 2N3 and doxylcyclohexane, indicated in Fig. 1. The methylene couplings are equivalent end-to-end and depend essentially only on their distance from the attachment point, even for spin probes with attachment points near the end. Figure 9 shows a map of the coupling constants in JN14 at 353 K. The dots mark the attachment point and the doxyl is omitted for clarity. The dashed line at the attachment point gives the coupling con-

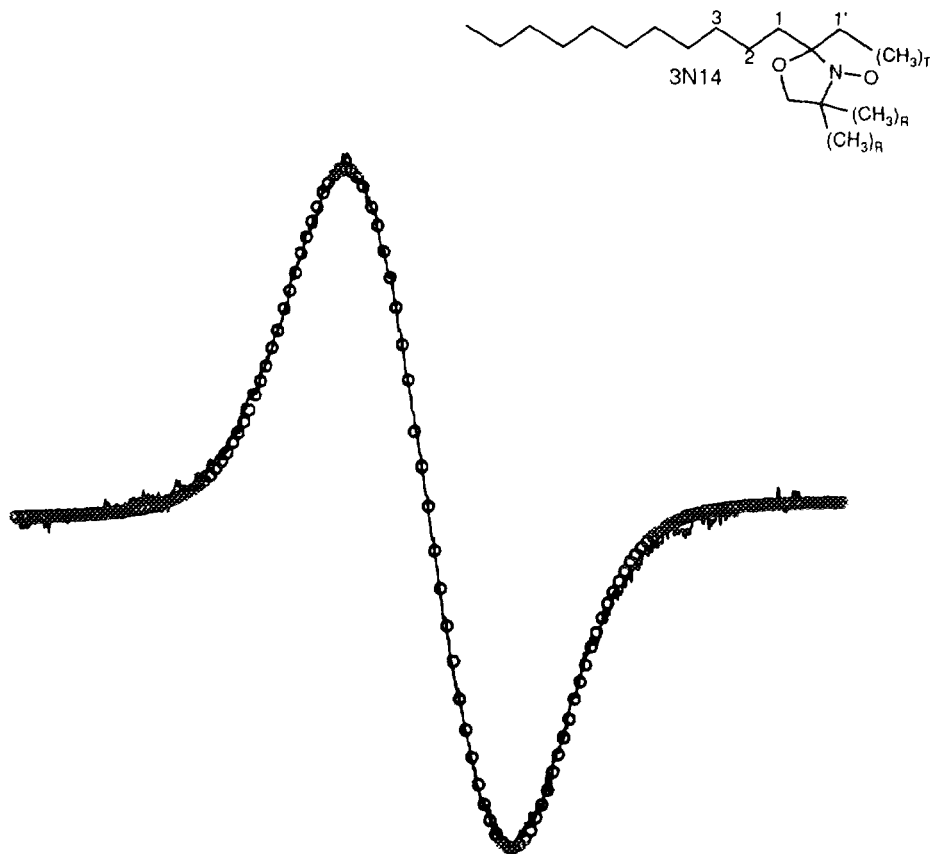


FIG. 7. EPR spectrum of the center line of 3N14 in toluene at 298 K. The circles show the simulation of the pattern predicted by the hyperfine coupling constants in Table 4 using  $\Delta H_{pp}^L = 0.18$  G. The overall linewidth of the spectral line is  $\Delta H_{pp}^0 = 0.94$  G, so ignoring the inhomogeneous broadening would lead to an error in the intrinsic width of more than 400%.

stant to  $(\text{CH}_3)_R$ . As the doxyl is moved to one end, the map remains very stable, even as  $(\text{CH}_3)_T$  couplings begin to appear. The impression from Fig. 9 is that  $(\text{CH}_3)_T$  enjoy the

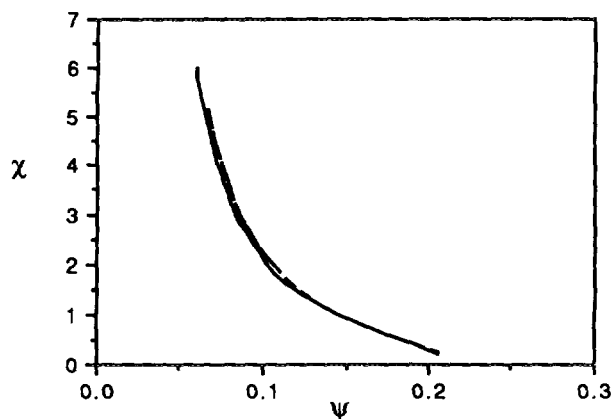


FIG. 8. Voigt parameter  $\chi = \Delta H_{pp}^S / \Delta H_{pp}^L$  vs the lineshape parameter,  $\psi$ . The spectrum in Fig. 7 is at  $\chi = 4.8$ , a value well above that at which almost all other spin probes show resolved proton hyperfine structure. The dashed line is a plot of Eq. [6].

spin density that was reserved for chain methylene protons in members of the series labeled toward the center. The coupling constants to protons attached to carbons adjacent to the attachment point are negative, and couplings to more distant groups are positive, even if these groups are  $(\text{CH}_3)_T$  ( $N = 2-4$ ). The negative coupling to  $(\text{CH}_3)_T$  is expected for 2N14 since it was found for 2N3 (Fig. 1n) and since  $(\text{CH}_3)_T$  is similar to the ring methyl group for 2N14. Note that the measurements yielding equivalent coupling constants in 2N3 (7) were made at 100 MHz; higher NMR frequencies uncover the inequivalence between  $(\text{CH}_3)_R$  and  $(\text{CH}_3)_T$  (12).

Forming the alkyl chain into a cyclic structure, (Figs. 1l and 1m) induces changes in the hyperfine couplings. The structure of doxycyclohexane has been rigorously determined (7) and a number of hyperfine splittings in doxycyclododecane have been identified by EPR and ENDOR (13). Protons adjacent to the attachment point in doxycyclohexane (Fig. 1m) are negative and show an inequivalence between the two on the same methylene, and the couplings on methylenes two bonds away are positive and again inequivalent. At room temperature or below, doxycyclododecane (Fig. 1l), shows a large (1.7–2.2 G) splitting to a single

TABLE 5  
Gaussian Linewidths Derived from NMR and EPR

Spin probe	Solvent	$T$ (K)	$\Delta H_{pp}^G$ (G) NMR <sup>a</sup>	$\Delta H_{pp}^G$ (G) EPR <sup>b</sup>
2N14	C <sub>6</sub> D <sub>6</sub>	296	0.603	0.716 ± 0.022 (6)
		323	0.628	
		353	0.647	
3N14	C <sub>6</sub> D <sub>6</sub>	296	0.873	0.845 ± 0.004 (4)
		323	0.869	
		353	0.879	
4N14	C <sub>6</sub> D <sub>6</sub>	296	0.799	0.790 ± 0.007 (3)
		323	0.794	
		353	0.799	
5N14	C <sub>6</sub> D <sub>6</sub>	296	0.792	0.795 ± 0.017 (3)
		323	0.791	
		353	0.800	
6N14	C <sub>6</sub> D <sub>6</sub>	296	0.799	0.814 ± 0.029 (3)
		323	0.794	
		353	0.801	
7N14	C <sub>6</sub> D <sub>6</sub>	296	0.799	0.803 ± 0.014 (7)
		323	0.784	
		353	0.771	
7N14	CD <sub>3</sub> OD	297	0.794	
		323	0.786	
16DSA	CCl <sub>3</sub> D	307	0.839	
		323	0.821	

<sup>a</sup> Uncertainty, estimated from the uncertainty in locating the resonance frequencies, ±6 mG,  $N = 3-7$ ; ±8 mG, 2N14; ±7 mG, 16DSA. Note that uncertainty due to temperature uncertainty is quite small due to the canceling of the temperature dependence of the hyperfine constants in Eq. [3], so these uncertainties are less than the square root of the sum of the squares in Table 2.

<sup>b</sup> Derived from least-squares fit of Gaussian/Lorentzian sum functions to the experimental spectra. Mean values and standard deviations from results in the number of measurements given in the parentheses.  $T = 298$  K.

proton on the methylene adjacent to the attachment point. This splitting disappears at high temperatures and shows a small increase with solvent polarity and a small decrease with rising temperature in analogy with the  $H_{L1}$  protons in the  $n$ -alkyl chains studied here. At high temperatures, the EPR could be simulated (13) with six coupling constants of 0.2 G which might correspond to  $(CH_3)_R$ . Seven distinct hyperfine coupling constants were measured with ENDOR, so doxylcyclododecane is complicated.

For the commonly used spin probes that are derivatives of stearic acid, these results are relevant as follows: 16DSA ↔ 3N14; 12DSA ↔ 7N14. 17DSA has been synthesized (24), which would correspond to 2N14. Other stearic acid and ester probes would presumably have hyperfine structures similar to those of 5N14, 6N14, and 7N14 since these structures do not change with position. The only worry would be the influence of the carboxyl group if the

doxyl group were attached too near that terminal group. EPR measurements yielded  $\Delta H_{pp}^G = 0.780 \pm 0.012$  G for 5DSA in CH<sub>3</sub>OH at 274 K (1), which is the same, within experimental error, as the values in Table 5 for 7N14 in CD<sub>3</sub>OD. This shows that the sum of the squares of the hyperfine cou-

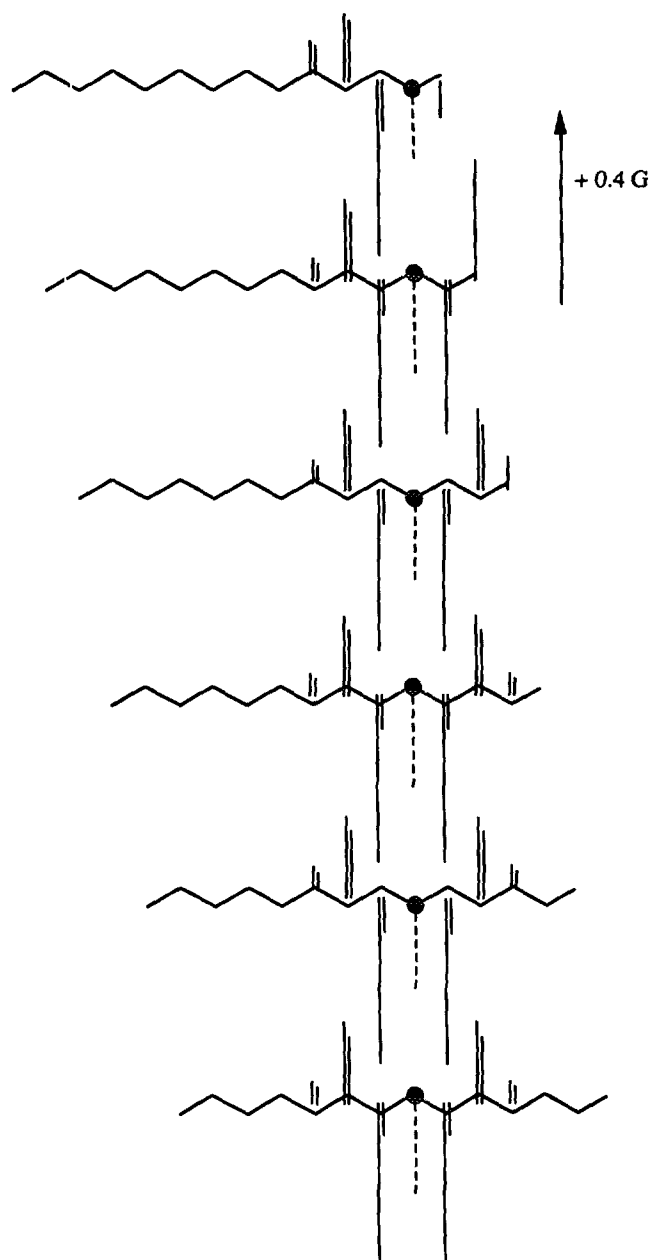
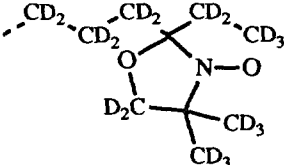
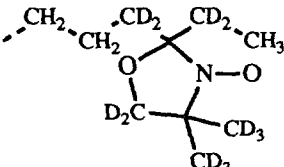
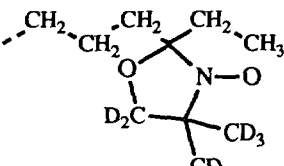
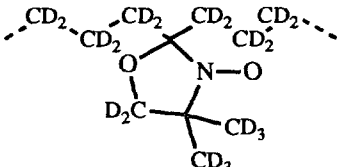
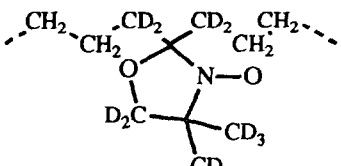


FIG. 9. Map of hyperfine coupling constants, magnitude and sign, in the series  $N14$  vs doxyl attachment position. The dotted line shows the hyperfine coupling constant to the ring methyl protons. The maps of the longer end of the chain are almost identical, even when the attachment point approaches the end of the spin probe. Selective deuteration to reduce the inhomogeneous broadening of the EPR spectra ought to extend to two carbons removed from the attachment site which includes the terminal methyl group in 3N14 ↔ 16DSA.

TABLE 6  
Effect of Selective Deuteration of Doxyl-Labeled *n*-Alkyl Chains

		$\Delta H_{pp}^L$	$\Delta H_{pp}^G$	$\Delta H_{pp}^{*G}$	$\Delta H_{pp}^0$	$\Delta H_{pp}^{*0}$	$V_{pp}^*/V_{pp}$
	Theory	0.185	0.870	0.218	0.97	0.33	5.3
	Theory	0.185	0.87	0.61	0.97	0.71	1.7
	Theory	0.185	0.87	0.82	0.97	0.97	1.1
	Theory Experiment <sup>a</sup>	0.241	0.790	0.201	0.92 1.00	0.35 0.38	3.8 3.7 <sup>b</sup>
	Theory Experiment <sup>c</sup>	0.24	0.79	0.36	0.92 1.0	0.50 0.67	2.5 1.3 <sup>d</sup>

Note. Linewidths are in gauss.

<sup>a</sup> Reference (28); 12DSA in water.

<sup>b</sup> The reported (28) factor of 5.5 divided by 1.5.

<sup>c</sup> Reference (29).

<sup>d</sup> The reported (29) factor 2.5 divided by 1.5.

pling constants (Eq. [3]) is the same for 7N14 and 5DSA. Therefore, it seems quite safe to use 7N14 parameters for all stearic acid and ester probes from 15DSA to 5DSA.

#### PREDICTING THE ADVANTAGES OF DEUTERATION OF *n*-ALKYL CHAINS

Deuterium substitution (25–27) yields gains in resolution and sensitivity because the smaller magnetic dipole moment of the deuteron reduces the hyperfine coupling constants and therefore reduces  $\Delta H_{pp}^G$  (Eq. [3]). The subject, from

the point of view of inhomogeneous line broadening, was discussed extensively previously (1). The question of proton contamination in selectively deuterated spin probes was also discussed previously (1); for simplicity, we assume perfect deuteration at the selected sites. In this section, we denote with an asterisk quantities related to a deuterated spin probe. Knowledge of the hyperfine structure permits the calculation of  $\Delta H_{pp}^{*G}$  by substituting  $a_j^* = \beta a_j$  in place of  $a_j$ ,  $\beta = (\gamma_D/\gamma_H)\sqrt{8/3} = 0.2507$ , where  $\gamma_D$  and  $\gamma_H$  are the gyromagnetic ratios of the deuteron and proton, respectively. Table 13 of Ref. (1) lists  $\Delta H_{pp}^{*G}$  in water for most of the

TABLE 7  
Gaussian Linewidths Derived from Eqs. [10] and [3], in Gauss

Spin probe	Solvent	$\Delta H_{pp}^0$	$\Delta H_{pp}^{*0}$	$\Delta H_{pp}^G$ Eq. [10]	$\Delta H_{pp}^G$ Eq. [3]	$\Delta H_{pp}^L$ <sup>a</sup>
12DSA <sup>b</sup>	H <sub>2</sub> O, 299 K	1.0	0.38	0.86	0.79 <sup>c</sup>	0.26
12DSA	H <sub>2</sub> O	1.0	0.44	0.81	0.79 <sup>c</sup>	0.35
2N3	DME <sup>d</sup>	0.75	0.71	0.18		0.71
2N3	CH <sub>3</sub> OH	0.70	0.58	0.30		0.57
2N3	CH <sub>3</sub> CH <sub>2</sub> OH	0.69	0.41	0.46		0.38
2N3	H <sub>2</sub> O	0.47	0.31	0.29		0.29
2N3	Cl <sub>3</sub> CD				0.451 <sup>e</sup>	
TEMPONE	DME	0.73	0.46	0.47	0.412 <sup>f</sup>	0.43
TEMPONE	CH <sub>3</sub> OH	0.70	0.45	0.45		0.42
TEMPONE	CH <sub>3</sub> CH <sub>2</sub> OH	0.60	0.36	0.40		0.33
TEMPONE	H <sub>2</sub> O	0.43	0.33	0.22	0.215 <sup>g</sup>	0.32
DTBN	DME	0.80	0.47	0.54	0.476 <sup>f</sup>	0.43
DTBN	CH <sub>3</sub> OH	0.59	0.42	0.33		0.40
DTBN	CH <sub>3</sub> CH <sub>2</sub> OH	0.54	0.40	0.29		0.39
DTBN	H <sub>2</sub> O	0.47	0.30	0.30	0.26 <sup>g</sup>	0.28
TEMPOL	DME	1.58	0.58	1.38	1.40 <sup>f</sup>	0.37
TEMPOL	CH <sub>3</sub> OH	1.52	0.57	1.32		0.38
TEMPOL	CH <sub>3</sub> CH <sub>2</sub> OH	1.50	0.53	1.33		0.32
TEMPOL	H <sub>2</sub> O	1.50	0.51	1.35	1.42 <sup>g</sup>	0.29

<sup>a</sup> From Eqs. [4] and [10].

<sup>b</sup> Reference (28).

<sup>c</sup> Average of measurements JN14,  $N = 4-7$ , in Cl<sub>3</sub>CD and CD<sub>3</sub>OD; Table 5 this work.

<sup>d</sup> Dimethoxyethane.

<sup>e</sup> From Eq. [3] using NMR data from Ref. (7).

<sup>f</sup> In CCl<sub>4</sub> from Eq. [3] using NMR and EPR data from Ref. (8).

<sup>g</sup> From Eq. [3] using NMR and EPR data from Ref. (8).

important classes of perfectly perdeuterated spin probes except for doxyl spin probes. Once  $\Delta H_{pp}^{*G}$  is predicted for a given selective deuteration,  $\chi^*$  may be calculated for a given  $\Delta H_{pp}^L$ . From  $\chi^*$ , all of the correction procedures of Ref. (1) become available. Of interest in some studies is the gain in line height,  $V_{pp}$ , obtained upon selective deuteration. If two samples have the same number of spins, then the doubly integrated first-derivative signals,  $A$ , are equal. Equating  $A$  given by Eq. [18] of Ref. (1) for deuterated vs protonated and solving for the ratio of the line heights gives

$$V_{pp}^*/V_{pp} = F(\Delta H_{pp}^0)^2 / F^*(\Delta H_{pp}^{*0})^2, \quad [7]$$

where  $F$  is a factor that depends on the lineshape as follows (1):

$$F = (1.03\chi^2 + 1.21\chi + 1.71) / (\chi^2 + 0.298\chi + 0.471). \quad [8]$$

For doxyl-labeled  $n$ -alkyl chains, Eq. [8] is directly applicable; for other spin probes, a correction factor is given

by Eq. [35] of Ref. (1). Unfortunately, the line height does not grow as fast upon deuteration (Eq. [7]) as the square of the linewidth ratios because the factor  $F$  increases as the line becomes more Lorentzian.

Table 6 shows some examples of predicted results of selective deuteration. The results depend on the Lorentzian linewidth; the values used correspond to those measured in this work at 298 K in toluene. Qualitatively, it is clearly of advantage to replace protons that have the largest hyperfine coupling constants. The first row of Table 6 shows the quantitative effect of perdeuterating 16DSA  $\leftrightarrow$  3N14. The overall linewidth is reduced by a factor of about 3 and the line height increases by a factor of 5. <sup>15</sup>N substitution would increase the line height by about another factor of 1.5 (28, 29), giving an overall increase of about 8. The second row shows that the advantage is quickly lost if (CH<sub>3</sub>)<sub>T</sub> and position 2 and 3 methylene protons are not replaced. The third row shows that it is almost a waste of effort to deuterate only the ring. The last two rows in Table 6 compare the predicted advantages with some experimental data in the literature (28, 29). Both <sup>15</sup>N and deuterons were substituted into 5DSA and 12DSA. In the former, (CH<sub>3</sub>)<sub>R</sub>, (CH<sub>2</sub>)<sub>R</sub>, and (CH<sub>2</sub>)<sub>1,1'</sub> pro-



tons were replaced while the latter was perdeuterated. We have made the approximation that  $^{15}\text{N}$  substitution increases the line height by 1.5, which is equivalent to assuming that  $\Delta H_{pp}^L$  is the same in the  $^{14}\text{N}$  and  $^{15}\text{N}$  spin probes. This is only approximately correct but probably satisfactory because factors near 1.5 were reported (28, 29) in cases involving only  $^{15}\text{N}$  substitution. With these caveats, we compare the reported vs predicted linewidth reductions and height enhancements for 12DSA and 5DSA in Table 6. Excellent agreement is found for the perdeuterated 12DSA. For 5DSA, both the height enhancement and the linewidth reduction are somewhat less than the predicted values.

For perfectly perdeuterated spin labels whose only significant source of inhomogeneous broadening is unresolved proton hyperfine structure,  $\Delta H_{pp}^{*G} = \beta \Delta H_{pp}^G$ , independent of the details of the structure (1). If only measurements of  $\Delta H_{pp}^0$  and  $\Delta H_{pp}^{*0}$  (no lineshape information) are available from EPR of the spin probe and the perdeuterated spin probe under identical conditions, then an estimate may be made of  $\Delta H_{pp}^G$  by assuming that  $\Delta H_{pp}^L$  is the same for both spin probes. Solving Eq. [4] for  $\Delta H_{pp}^L$  for deuterated vs protonated probes and equating yield

$$\Delta H_{pp}^0 [1 - (\Delta H_{pp}^G / \Delta H_{pp}^0)^2] = \Delta H_{pp}^{*0} [1 - (\Delta H_{pp}^{*G} / \Delta H_{pp}^{*0})^2]. \quad [9]$$

Inserting  $\Delta H_{pp}^{*G} = \beta \Delta H_{pp}^G$  and solving for  $\Delta H_{pp}^G$  yield

$$\Delta H_{pp}^G = \sqrt{\frac{\Delta H_{pp}^0 - \Delta H_{pp}^{*0}}{1/\Delta H_{pp}^0 - \beta^2/\Delta H_{pp}^{*0}}}. \quad [10]$$

Table 7 gives some results taken from the literature, including perdeuterated 12DSA discussed above. For 12DSA, TEMPONE, DTBN, and TEMPOL, the agreement between NMR results (Eq. [3]) and the results deduced from EPR using Eq. [10] are quite good. The results for 2N3 are not very consistent; Eq. [10] gives  $\Delta H_{pp}^G = 0.30 \pm 0.11$  G in four solvents while  $\Delta H_{pp}^G = 0.451$  G from NMR.

#### ACKNOWLEDGMENTS

This work was supported by the U.S. Army Research Office Grant DAALO 3-88-K-0006. We are grateful for the use of the Cal. Tech. NMR regional facility, sponsored by the NSF (Grant CHE 84-40137). Useful discussions with Professors J. Hajdu and E. Rosenberg are gratefully acknowledged.

#### REFERENCES

1. B. L. Bales, in "Biological Magnetic Resonance" (L. J. Berliner and J. Reuben, Eds.), Vol. 8, p. 77, Plenum, New York, 1989.
2. R. Brière, J. Lemaire, A. Rassat, P. Rey, and A. Pousseau, *Bull. Soc. Chim. Fr.*, 4479 (1967).
3. R. Brière, H. Lemaire, A. Rassat, and J. Dunand, *Bull. Soc. Chim. Fr.* 4220 (1970).
4. R. W. Kreilick, *J. Chem. Phys.* **45**, 1922 (1966).
5. R. W. Kreilick, *J. Chem. Phys.* **46**, 4260 (1967).
6. P. Michon and A. Rassat, *J. Org. Chem.* **39**, 2121 (1971).
7. P. Michon and A. Rassat, *Bull. Chim. Soc. Fr.*, 3561 (1971).
8. J. J. Windle, *J. Magn. Reson.* **45**, 432 (1981).
9. F. B. Barbarin, B. Chevarin, J. P. Germain, C. Fabre, and D. Cabaret, *Mol. Cryst. Liq. Cryst.* **46**, 181 (1978).
10. F. B. Barbarin, B. Chevarin, J. P. Germain, C. Fabre, and D. Cabaret, *Mol. Cryst. Liq. Cryst.* **46**, 195 (1978).
11. B. L. Bales, R. A. Blum, D. Mareno, M. Peric, and H. Halpern, *J. Magn. Reson.* **98**, 299 (1992).
12. J. Dunand, *C. R. Acad. Sci. Paris* **267**, 82 (1968).
13. S. S. Eaton, H. V. Willigen, M. J. Heinig, and G. R. Eaton, *J. Magn. Reson.* **38**, 325 (1980).
14. S. N. Dobryakov and Y. S. Lebedev, *Sov. Phys. Dokl.* **13**, 873 (1969).
15. H. J. Halpern, M. Peric, C. Yu, and B. L. Bales, *J. Magn. Reson.*, in press.
16. J. Carson, *Chem. Rev.* **40**, 15 (1947).
17. W. L. Hubbell and H. M. McConnell, *J. Am. Chem. Soc.* **93**, 314 (1971).
18. S. J. Cristol, *J. Org. Chem.* **26**, 280 (1961).
19. J. F. W. Keana, S. B. Keana, and D. Beetham, *J. Am. Chem. Soc.* **89**, 3055 (1967).
20. A. R. Katritzky and A. P. Amplier, in "Physical Methods in Heterocyclic Chemistry" (A. R. Katritzky, Ed.), Vol. 2, p. 161, Academic Press, New York, 1963.
21. D. Mareno, Master of Science Thesis, California State University at Northridge, 1991.
22. U. M. Oehler and E. G. Janzen, *Can. J. Chem.* **60**, 1542 (1982).
23. B. L. Bales, K. Schumacher, and F. L. Harris, *J. Phys. Chem.* **91**, 1701 (1987).
24. J. J. Windle, private communication.
25. R. Chiarelli and A. Rassat, *Tetrahedron* **29**, 3639 (1973).
26. J. S. Hwang, R. P. Mason, L. Hwang, and J. H. Freed, *J. Phys. Chem.* **79**, 489 (1975).
27. S. Lee and A. Shetty, *J. Chem. Phys.* **83**, 499 (1985).
28. S. D. Venkataramu, D. E. Pearson, A. H. Beth, C. R. Park, and J. H. Park, *Tetrahedr. Lett.* **26**, 1403 (1985).
29. J. H. Park and W. E. Trommer, in "Biological Magnetic Resonance" (L. J. Berliner and J. Reuben, Eds.), Vol. 8, p. 547, Plenum, New York, 1989.
30. F. Baykut and S. Ozeris, *Rev. Fac. Sci. Univ. Istanbul* **21**, 102 (1956).